

Phonon dynamics of single nanoparticles studied using confocal pump-probe backscattering

Kung-Hsuan Lin (林宮玄),^{1,a)} Hao-Yu Cheng (鄭皓宇),¹ Chi-Yuan Yang (楊濟源),^{1,2} Hung-Wei Li (李泓緯),³ Chih-Wei Chang (張之威),³ and Shi-Wei Chu (朱士維)^{2,4,a)}

¹*Institute of Physics, Academia Sinica, Taipei 11529, Taiwan*

²*Department of Physics, National Taiwan University, Taipei 10617, Taiwan*

³*Center for Condensed Matter Sciences, National Taiwan University, Taipei 10617, Taiwan*

⁴*Molecular Imaging Center, National Taiwan University, Taipei 10617, Taiwan*

(Received 17 July 2018; accepted 9 October 2018; published online 23 October 2018)

Confocal pump-probe backscattering was used to study phonon dynamics of single nanoparticles, which can extend to confocal pump-probe microscopy for investigating carrier dynamics of single nanomaterials. Compared to previous pump-probe microscopy studies, in which nonlinear optical generation was widely utilized, spectral filters were employed in this work to separate the spectra from the optical pulses for pump/probe beams. This not only reduces the complexity of the experimental setup but can also circumvent the aberration issue. Phonon dynamics, including acoustic vibrations and heat diffusion, of a single gold nanoparticle were measured with a temporal delay of 8 ns, and a 0.5 K rise in the temperature of the surrounding media was resolved. The relative optical changes induced by the photoexcitation of the pump pulses in confocal reflection pump-probe traces were orders of magnitude larger than those in typical transmission-type pump probe traces. *Published by AIP Publishing.* <https://doi.org/10.1063/1.5048669>

Ultrafast optical spectroscopy is a convenient and powerful tool to study the dynamics of carriers (such as electrons and phonons) with subpicosecond time scales. For conventional pump-probe techniques, the optical spot sizes on the samples are typically in the range between 10 μm and several hundreds of micrometers. Thus, it is common to assume that the carrier dynamics are homogeneous within the probing area. In recent decades, however, many materials, such as nanomaterials and 2D materials, have emerged that are spatially inhomogeneous. Integration between ultrafast spectroscopy and optical microscopy has thus been developed for such materials.^{1–16}

In this work, we demonstrated a technique that enables confocal pump-probe microscopy for studying phonon dynamics of single nanoparticles. First, sharp spectral filters were used to separate the spectra from the same optical pulses to create a pump beam and a probe beam. Previously, nonlinear optical generation was widely utilized to separate spectrally the pump/probe beams in a microscope.^{1–22} However, the chromatic aberration of a high-NA objective lens becomes a serious issue when the wavelengths of the pump/probe beams are far from each other. In the setup used, the wavelengths of pump/probe beams were close, and the aberration effect was minimized, because their spectra were directly divided from the full bandwidth of the original pulses. Compared with nonlinear generation, spectral filters could also reduce the complexity of the experimental setup. Second, a confocal backscattering scheme was utilized for measuring isolated single nanoparticles. In contrast to the widely used transmission pump-probe microscopy, the confocal scheme provided axial sectioning capability, which

confined the detection volume down to subfemtoliter when combined with a tightly focusing objective. Third, the relative optical changes induced by the photoexcitation of the pump pulses ($\Delta S/S$ is $\sim 10^{-3}$, where S is the total intensity of the scattered probe at the detector) in confocal reflection pump-probe traces were orders of magnitude larger than those in typical transmission-type pump-probe traces ($\Delta Tr/Tr$ is $\sim 10^{-5}$, where Tr is the total intensity of the transmitted probe at the detector). Because the size of optical spots at focus is larger than the cross sectional area of single nanoparticles, light without interacting with the nanoparticle contributes strong background signals in Tr , leading to much reduced $\Delta Tr/Tr$. In contrast, light collected by the detector in the confocal reflection mode is dominated by backscattering from the nanoparticle embedded in the index-matching matrix. The optical changes $\Delta S/S$ in a confocal reflection setup could thus be much larger than $\Delta Tr/Tr$ in a transmission setup.

To demonstrate this technique, carrier dynamics of single gold nanoparticles up to 8 ns were studied by using a Ti:sapphire oscillator with a 12.5-ns repetition period. Figure 1(a) shows the spectra of the optical pulses in a black solid line. The central wavelength is 785 nm with a full-width-at-half-maximum (FWHM) of ~ 12 nm. The reader is referred to the [supplementary material](#) to see the detailed schematic and description of the experimental setup. A long-wave-pass filter and a short-wave-pass filter were inserted into the pump and probe beam paths, respectively, to block the long-wavelength part and short-wavelength part of the laser pulses with a bandwidth of 12 nm. The red and blue lines in Fig. 1(a) indicate that the reshaped spectra did not overlap in wavelength. Figure 1(b) shows the cross-correlation of the optical pump and probe pulses in the time domain. A beta barium borate (BBO) crystal was used to record the second-harmonic generation as a

^{a)} Authors to whom correspondence should be addressed: linkh@sinica.edu.tw and swchu@phys.ntu.edu.tw

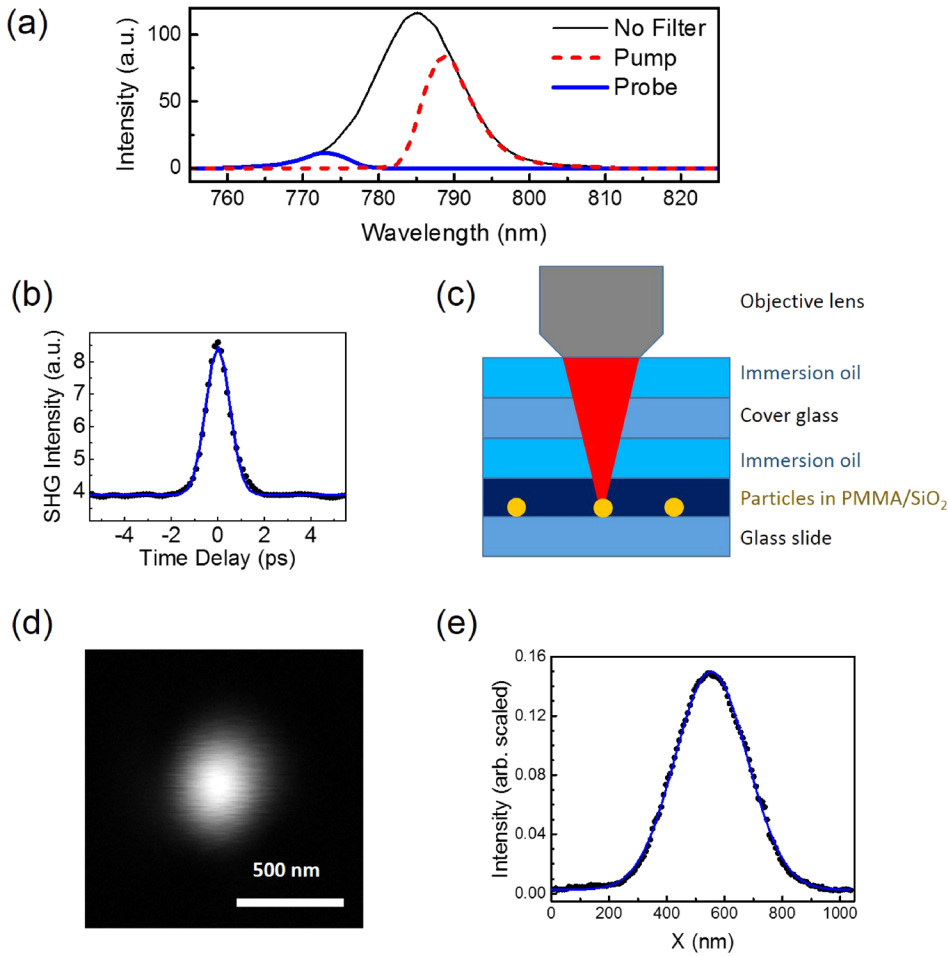


FIG. 1. (a) Spectra of the laser pulses (black solid line) and spectra after the laser pulses pass through a long-wave-pass filter for the pump (red dashed line) and a short-wave-pass filter for the probe (blue solid line), (b) cross-correlation of the pump-probe pulses in the time domain by using second-harmonic generation, (c) schematic of the sample structures, (d) typical confocal image of a single gold nanoparticle (the brightness indicates the intensity of the backscattered light), and (e) the line profile, which crossed the center of the particle in (d).

function of pump-probe delay. The FWHM of the cross-correlation response was approximately 1 ps, indicating the temporal resolution. Figure 1(c) shows the structure of the samples. Two sets of gold nanoparticles (purchased from BBI Solutions) were prepared for measurements. Sample A was specified as 80 nm in diameter with 10% variation, and sample B was specified as 150 nm in diameter with 10% variation. The gold nanoparticles were first dispersed on the glass slides and then coated with the poly(methyl methacrylate) (PMMA) film (sample A) and SiO₂ film (sample B), respectively. Immersion oil was dropped on the films, and a cover glass was placed on top. Figure 1(d) shows the typical confocal image of a gold nanoparticle. The individual nanoparticles were well separated with intervals of at least several micrometers, although some aggregates were observed in the confocal images (not shown here). The corresponding FWHM of the image in Fig. 1(e) was ~ 300 nm, which agrees well with the diffraction limit $\lambda/2NA$.

After a gold nanoparticle was identified at a confocal image, the galvo mirrors were used to point the collinear pump/probe beam onto the center of the gold nanoparticle, and the intensity changes of the scattered probe beam ($\Delta S/S$) were recorded as a function of time delay. After the pump pulses excited electrons in the gold nanoparticle, the energy of hot electrons dissipated through electron–electron scatterings and electron–phonon scatterings.²³ The electron and lattice temperatures reached equilibrium on the timescale of picoseconds, and the subsequent phenomena were observed, including a transient thermal energy that initiated the

acoustic vibration of the gold nanoparticle followed by heat transfer from the gold nanoparticle into the surrounding media. The black line in Fig. 2(a) shows the scattering changes as a function of time delay for sample A. To obtain quantitative features, the experimental data were phenomenologically fitted with the following equation:

$$\frac{\Delta S(t)}{S} = A_0 U(t) + A_1 \exp\left(-\frac{t}{\tau_1}\right) U(t) + A_S \exp\left(-\frac{t}{\tau_S}\right) \sin[2\pi f_S(t - t_S)] U(t), \quad (1)$$

where $U(t)$ is the step function. The first term on the right-hand side of Eq. (1) describes the slow relaxation with a time constant much longer than the observation time. The second term is an exponential decay function for the background relaxation. The third term describes the oscillation component with an exponential damping. The fitting results are summarized in Table I, and the fitting curve is revealed with a blue line in Fig. 2(a). The oscillation frequency f_S is 15.5 GHz with damping time $\tau_S = 200$ ps. The relaxation time of the background τ_1 is 384 ps, which reflects the characteristic time of thermal diffusion. Similarly, Fig. 2(b) shows the results for sample B. As shown in Table I, an oscillation frequency $f_S = 7.4$ GHz was obtained with damping time $\tau_S = 472$ ps. Compared with Figs. 2(a) and 2(b) for samples A and B, there are three primary features for the optical probe changes after photoexcitation of the pump pulses. First, Fig. 2(a) exhibits a transient positive response,

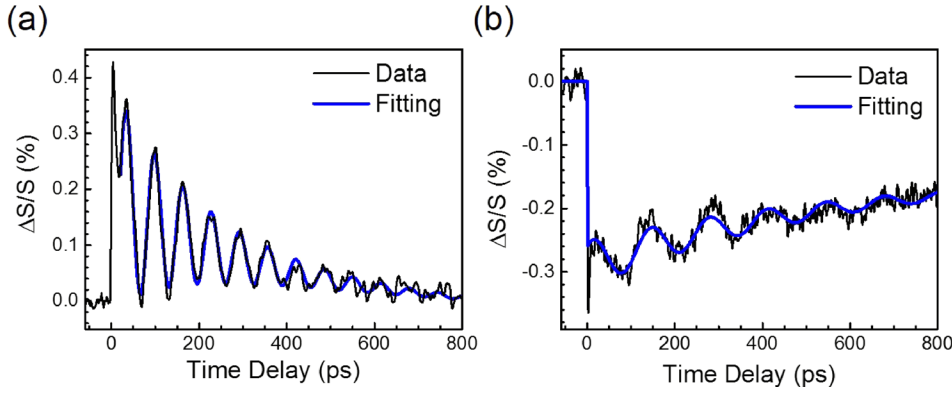


FIG. 2. Pump-probe traces of single gold nanoparticles covered by (a) PMMA (sample A) and (b) silica films (sample B): the frequency of oscillations indicates that the diameters of the particles are (a) 77 nm and (b) 162 nm, respectively.

TABLE I. Fitting parameters in Eq. (1) of each figure.

Figure	$A_0(\times 10^{-4})$	$A_1(\times 10^{-4})$	τ_1	$A_S(\times 10^{-4})$	τ_S	f_S	t_S
2(a)	-1.9	20.8	384 ps	20	200 ps	15.5 GHz	1.75 ps
2(b)	-14.1	-14.8	612 ps	-3.7	472 ps	7.4 GHz	-0.89 ps
4(a)	None	-3	2.5 ns	None	None	None	None
4(b)	-1.6	-18.5	3.9 ns	None	None	None	None

while the other is a transient negative response. Second, the oscillation frequency of sample A (with a particle size of ~ 80 nm) is higher than that of sample B (with a particle size of ~ 150 nm). Finally, the background relaxation in Fig. 2(a) is faster than that in Fig. 2(b). The three features are further discussed sequentially.

The changes of optical scattering arise from the plasmonic effect, which is associated with the complex refractive index n_G of gold, the refractive index of surrounding media n_S , and the diameter of the gold sphere d . The optical scattering by small particles can be calculated based on Mie theory.²⁴ The cross-sectional area for scattering C_S can be approximated as²⁴

$$C_S = \frac{\pi}{24} d^6 k^4 \left| \frac{\varepsilon_G - \varepsilon_S}{\varepsilon_G + 2\varepsilon_S} \right|^2 \quad \text{if } kd = 1. \quad (2)$$

Here, k is the wavevector of light, $\varepsilon_G = n_G^2$, and $\varepsilon_S = n_S^2$. The optical intensity of scattering (S) can thus be changed by any parameter on the right-hand side of Eq. (2). The calculated spectra of C_S (without approximation of $kd = 1$) are shown in Figs. 3(a) and 3(b). The resonance peaks are 585 nm and 740 nm for $d = 77$ nm and $d = 162$ nm, respectively. Previous reports^{3,4} indicate that the optical changes in the

pump-probe traces are dominated by the variations of n_G , which are associated with the temperature evolution of the gold nanoparticle. The changes of n_G modify the spectra of scattering in Fig. 3. C_S increases on the red side, while it decreases on the blue side.⁴ The crossing point of sign changes is a couple tens of nanometers on the red side of the resonant peak.⁴ As shown in Fig. 3(a), the probe wavelength of ~ 785 nm is far longer than the resonant wavelength of sample A. The positive sign of optical changes in Fig. 2(a) agrees with previous reports.⁴ For sample B, the probe wavelength is close to the resonant wavelength as shown in Fig. 3(b). Although the probe wavelength is still on the red side of the resonance peak, the negative sign in Fig. 2(b) indicates that the probe wavelength is already shorter than the aforementioned crossing point.

Second, the photoexcited acoustic waves (i.e., mechanical vibrations of the gold nanoparticle) can alter the refractive index and the size of the gold nanoparticle. The scattering spectrum, because of the plasmonic effects, is thus modulated, leading to oscillations of scattering intensity at the probe wavelength. According to Lamb's work,²⁵ the vibrational modes of an elastic sphere are categorized into spheroidal modes and torsional modes. Lamb denoted the spheroidal modes with two integer parameters (n, l),²⁵ where n is the solution number and l is the angular momentum number. The lowest mode (0, 0) is known as the radial breathing mode, and the frequency $f = v_L/d$,^{25,26} where v_L is the longitudinal velocity and d is the diameter. This mode was widely observed in gold nanoparticles excited by pulsed lasers.^{2,4,18} The longitudinal velocity of gold, $v_L = 3240$ m/s,²⁷ leads to an expected frequency of 40.5 GHz for $d = 80$ nm. However, what was found in Fig. 2(a) is 15.5 ± 1 GHz, much smaller than the radial breathing frequency.

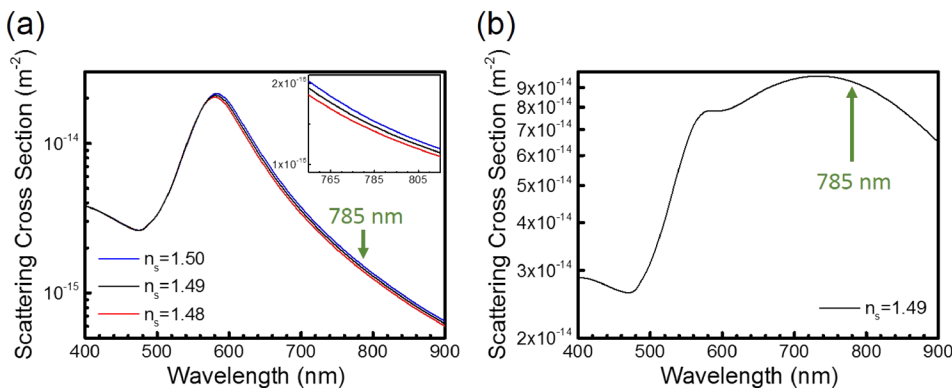


FIG. 3. Calculated scattering cross section of a gold sphere with diameters of (a) 77 nm and (b) 162 nm in surrounding media with a refractive index of 1.49 (black lines); (a) and the inset additionally indicates the scattering cross section in surrounding media with refractive indices of 1.50 (blue lines) and 1.48 (red lines).

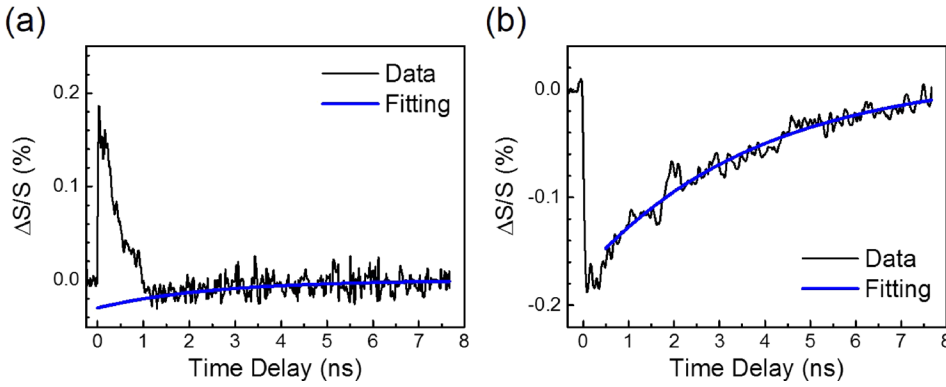


FIG. 4. Pump-probe traces of the same single gold nanoparticles in Fig. 2 with the time window up to 8 ns: the heat diffusion time of (a) the particle 77 nm in diameter is shorter than that of (b) the particle 162 nm in diameter.

A closer investigation leads to the possibility of observing the elliptical mode [or (0, 2) mode]. Unlike the radial breathing mode in which the sphere expands and shrinks obeying spherical symmetry, the elliptical mode has at least two basic axes of the sphere oscillating out of phase. That is, the sphere expands along one axis while it shrinks along another axis. The frequency of the elliptical mode $f = v_T/d$, where v_T is the transverse velocity.^{25,26} According to the transverse velocity of gold, $v_T = 1200$ m/s,²⁸ the frequency is 15 GHz for $d = 80$ nm. This value is close to what was found in Fig. 2(a). Therefore, the oscillations in Fig. 2(a) are attributed to the elliptical mode. The frequency distribution of the experimental data reflects the size distribution of the nanoparticles. From Fig. 2(a), with a 1200-m/s acoustic velocity and a 15.5-GHz oscillation frequency, the diameter of the particle can be estimated as 77 nm. Similarly, the observed frequency of 7.4 GHz in Fig. 2(b) was attributed to the elliptical mode, and the experimentally deduced diameter was 162 nm. Both the experimentally obtained sizes of gold nanoparticles are well within the size distribution (10%) in the specification provided by the supplier.

Previous studies⁴ observed that the breathing mode and elliptical mode of 80-nm gold nanoparticles coexisted, and their amplitudes were comparable in the Fourier spectra. Interestingly, the elliptical mode of the gold nanoparticles overwhelmed other modes, including the radial breathing mode. One possible explanation is that the nanoparticle is sandwiched by the bottom glass slide and the upper PMMA/silica film, which causes broken inversion symmetry. Indeed, the acoustic impedances of PMMA and fused silica are 3.25 and 13.15 MRaysls, respectively.²⁹ The large difference of elastic properties between the materials breaks the symmetry along the axial (z) direction, leading to the dominating elliptical mode rather than the radial breathing mode.

Finally, the background relaxation curves in Fig. 2 reflect the changes of n_G and n_S due to the temporal variations of temperature and are actually dominated by the temperature of the gold nanoparticle.³ It is estimated that 20 fJ from an optical pulse was absorbed by a 77-nm gold nanoparticle (sample A) if an absorption cross section 4×10^{-16} m² derived from the calculations of Mie theory is assumed. Because the thermal conductivity of gold is much higher than that of the surrounding media, the initial temperature rise of the 77-nm gold nanoparticle in Fig. 2(a) is estimated to be 40 K by assuming homogenous heating inside the gold nanoparticle with a heat capacity of 2.5×10^6 J m⁻³ K⁻¹. The temperature of the gold

nanoparticle subsequently decreases when heat propagates through the interface between the nanoparticle and its surrounding media. Although the curve in Fig. 2(a) seems to be decaying to zero within the time window of 800 ps, a slow and negative response in the background was found if the time window was extended up to 8 ns, as shown in Fig. 4(a). The fitting results, as summarized in Table I, indicate that $A_1 = -3 \times 10^{-4}$ with time constant $\tau_1 = 2.5$ ns. The negative response, which has never been found before,³ is evident in the experiment and analysis for the improved $\Delta S/S \sim 10^{-4}$.

Previous studies reported that the temperature dependence of the refractive index at room temperature is $dn_S/dT = -1.4 \times 10^{-4}$ K⁻¹ for PMMA.³⁰ The refractive index of PMMA decreases with increasing temperature T , and the variation is relatively large. The inset of Fig. 3(a) highlights the difference of the scattering cross section with $n_S = 1.50$ (in blue lines), $n_S = 1.49$ (in black lines), and $n_S = 1.48$ (in red lines), which indicates that the drop of n_S reduces the scattering cross section around 785 nm. This negative response $A_1 \exp(-t/\tau_1)$ in Fig. 4(a) is attributed to the change of n_S , caused by the temperature rise of the surrounding medium, PMMA. From the calculation of Mie theory in Fig. 3(a), the scattering cross section $C_S = 1.48 \times 10^{-15}$ m² at 785 nm with $n_S = 1.49$ at room temperature and $dC_S/dn_S = -6 \times 10^{-15}$ m². Because the scattering intensity S from the particle is proportional to the cross-section of scattering C_S in a confocal reflection configuration, the total intensity modulation of the probe ($\Delta S/S$) can be expressed as

$$\frac{\Delta S}{S} = \frac{\Delta C_S}{C_S} = \frac{1}{C_S} \frac{dC_S}{dn_S} \frac{dn_S}{dT} \Delta T. \quad (3)$$

According to Eq. (3), the initial temperature rise of the PMMA near the gold surface was thus estimated as $\Delta T \sim 0.5$ K for the negative response $\Delta S(t)/S = A_1 \exp(-t/\tau_1)$ in Fig. 4(a), where $A_1 = -3 \times 10^{-4}$, as listed in Table I. Therefore, the scattering signal in Fig. 4(a) was dominated by the temperature in the gold nanoparticle decreasing from 40 K to 0.5 K before 1 ns. Afterward, the scattering signal was dominated by the heat diffusion in the surrounding media.

Figure 4(b) shows the long traces of the 162-nm single gold particles covered with the silica film. A significant decay behavior can be observed within the 8-ns time window, and a fitting time constant of 3.9 ns is obtained (see Table I). This relaxation component corresponds to the aforementioned fitted step function $A_0 U(t)$ in Fig. 2(b),

because 3.9 ns is much longer than the time window of 800 ps. Compared with Figs. 2(a) and 4(a), the sign is negative in Figs. 2(b) and 4(b), because the probe wavelength is close to the scattering resonance of sample B, as discussed previously. In addition to the signals reflecting the time-resolved changes of n_G due to the temperature of gold, the signals due to heating of surrounding media were estimated, which are the negative slow relaxation following the positive fast relaxation in Fig. 4(a). For silica in sample B, the temperature dependence of the refractive index was $dn_S/dT = 1.3 \times 10^{-5} \text{ K}^{-1}$ at room temperature.³¹ According to the calculations at 785 nm, $dC_S/dn_S = -6.3 \times 10^{-14} \text{ m}^2$. Also, $d/dT(\Delta C_S/C_S) = 8.9 \times 10^{-6} \text{ K}^{-1}$, which is far smaller than that of PMMA in sample A ($4.2 \times 10^{-4} \text{ K}^{-1}$). The whole relaxation curves in Fig. 4(b) should be dominated by the thermal relaxation of the gold nanoparticle. Although the fitting, with two exponential decay functions with time constants of 612 ps and 3.9 ns (in Table I), is not based on the analytical solution, it was observed that the thermal relaxation time for the 162-nm gold nanoparticle was longer than that for the 77-nm one. This trend agrees with the experimental reports in the literature.^{3,32,33}

In summary, the advantages of investigating phonon dynamics with confocal pump-probe microscopy were demonstrated. Acoustic vibrations of gold nanoparticles were measured, and the heat diffusion process after single gold nanoparticles were heated by a pump beam was studied. Because of the extended observation window and the confocal setup, signals were observed due to the temperature evolution of the surrounding media, in addition to the common heat conduction of a single nanoparticle.

See [supplementary material](#) for the detailed schematic and description of the experimental setup.

The authors are grateful to acknowledge Yu-Ting Chen, Sheng-Yang Tsui, Po-Hsuan Lee, and Hsuan Lee for integrating the microscopy system. This work was sponsored by the Ministry of Science and Technology of Taiwan under Grant Nos. 104-2112-M-001-048-MY3, 105-2628-M-002-010-MY4, 107-2321-B-002-009, and 107-2119-M-001-046. S.-W.C. acknowledges the generous support from the Foundation for the Advancement of Outstanding Scholarship.

¹S. Berciaud, L. Cognet, G. A. Blab, and B. Lounis, *Phys. Rev. Lett.* **93**, 257402 (2004).

²M. A. van Dijk, M. Lippitz, and M. Orrit, *Phys. Rev. Lett.* **95**, 267406 (2005).

- ³V. Juve, M. Scardamaglia, P. Maioli, A. Crut, S. Merabia, L. Joly, N. Del Fatti, and F. Vallee, *Phys. Rev. B* **80**, 195406 (2009).
- ⁴A. L. Tchebotareva, P. V. Ruijgrok, P. Zijlstra, and M. Orrit, *Laser Photonics Rev.* **4**, 581 (2010).
- ⁵J. Cabanillas-Gonzalez, G. Grancini, and G. Lanzani, *Adv. Mater.* **23**, 5468 (2011).
- ⁶M. Domke, S. Rapp, M. Schmidt, and H. P. Huber, *Opt. Express* **20**, 10330 (2012).
- ⁷T. Virgili, G. Grancini, E. Molotokaite, I. Suarez-Lopez, S. K. Rajendran, A. Liscio, V. Palermo, G. Lanzani, D. Polli, and G. Cerullo, *Nanoscale* **4**, 2219 (2012).
- ⁸W. J. Choi, S. Y. Ryu, J. K. Kim, J. Y. Kim, D. U. Kim, and K. S. Chang, *Opt. Lett.* **38**, 4907 (2013).
- ⁹J. Y. Huang, J. Park, W. Wang, C. J. Murphy, and D. G. Cahill, *ACS Nano* **7**, 589 (2013).
- ¹⁰S. S. Lo, H. Y. Shi, L. B. Huang, and G. V. Hartland, *Opt. Lett.* **38**, 1265 (2013).
- ¹¹M. Seo, S. Boubanga-Tombet, J. Yoo, Z. Ku, A. V. Gin, S. T. Picraux, S. R. J. Brueck, A. J. Taylor, and R. P. Prasankumar, *Opt. Express* **21**, 8763 (2013).
- ¹²J. P. He, J. Miyazaki, N. Wang, H. Tsurui, and T. Kobayashi, *Opt. Express* **23**, 9762 (2015).
- ¹³S. Mezil, P. H. Otsuka, S. Kaneko, O. B. Wright, M. Tomoda, and O. Matsuda, *Opt. Lett.* **40**, 2157 (2015).
- ¹⁴J. Miyazaki, H. Tsurui, K. Kawasumi, and T. Kobayashi, *Opt. Express* **23**, 3647 (2015).
- ¹⁵D. Davydova, A. de la Cadena, D. Akimov, and B. Dietzek, *Laser Photonics Rev.* **10**, 62 (2016).
- ¹⁶J. Wu, D. Xiang, G. Hajisalem, F. C. Lin, J. S. Huang, C. H. Kuo, and R. Gordon, *Opt. Express* **24**, 23747 (2016).
- ¹⁷T. Feurer, J. C. Vaughan, and K. A. Nelson, *Science* **299**, 374 (2003).
- ¹⁸M. Pelton, J. E. Sader, J. Burgin, M. Z. Liu, P. Guyot-Sionnest, and D. Gosztola, *Nat. Nanotechnol.* **4**, 492 (2009).
- ¹⁹Q. Wu, C. A. Werley, K. H. Lin, A. Dorn, M. G. Bawendi, and K. A. Nelson, *Opt. Express* **17**, 9219 (2009).
- ²⁰K. Yu, P. Zijlstra, J. E. Sader, Q. H. Xu, and M. Orrit, *Nano Lett.* **13**, 2710 (2013).
- ²¹A. Ahmed, M. Pelton, and J. R. Guest, *ACS Nano* **11**, 9360 (2017).
- ²²C. P. Pan, Q. Wu, Q. Zhang, W. J. Zhao, J. W. Qi, J. H. Yao, C. L. Zhang, W. T. Hill, and J. J. Xu, *Opt. Express* **25**, 9768 (2017).
- ²³C. K. Sun, F. Vallee, L. Acioli, E. P. Ippen, and J. G. Fujimoto, *Phys. Rev. B* **48**, 12365 (1993).
- ²⁴C. F. Bohren and D. R. Huffman, *Absorption and Scattering of Light by Small Particles* (Wiley, New York, 1983).
- ²⁵H. Lamb, *Proc. London Math. Soc.* **s1-13**, 189 (1881).
- ²⁶E. Duval, A. Boukenter, and B. Champagnon, *Phys. Rev. Lett.* **56**, 2052 (1986).
- ²⁷R. E. Green, A. S. Birks, and P. MacIntire, *Nondestructive Testing Handbook, Ultrasonic Testing Vol. 7* (American Society for Nondestructive Testing, Columbus, OH, 1991).
- ²⁸D. E. Gray and B. H. Billings, *American Institute of Physics Handbook* (McGraw-Hill, New York, 1963).
- ²⁹G. Destgeer, J. H. Jung, J. Park, H. Ahmed, K. Park, R. Ahmad, and H. J. Sung, *RSC Adv.* **7**, 22524 (2017).
- ³⁰P. Michel, J. Dugas, J. M. Cariou, and L. Martin, *J. Macromol. Sci., Part B: Phys.* **25**, 379 (1986).
- ³¹T. Toyoda and M. Yabe, *J. Phys. D: Appl. Phys.* **16**, L97 (1983).
- ³²M. Hu, X. Wang, G. V. Hartland, V. Salgueirino-Maceira, and L. M. Liz-Marzan, *Chem. Phys. Lett.* **372**, 767 (2003).
- ³³Z. B. Ge, Y. J. Kang, T. A. Taton, P. V. Braun, and D. G. Cahill, *Nano Lett.* **5**, 531 (2005).